Particle separation by external fields on periodic surfaces

Particle separation by external fields on periodic surfaces

J M Sancho[1,4]**, M Khoury**[1]**, K Lindenberg**[2] **and A M Lacasta**[3]

[1] Departament d'Estructura i Constituents de la Matèria, Facultat de Física, Universitat de Barcelona, Diagonal 647, E-08028 Barcelona, Spain
[2] Department of Chemistry and Biochemistry 0340, and Institute for Nonlinear Science, University of California, San Diego, La Jolla, CA 92093-0340, USA
[3] Departament de Física Aplicada, Universitat Politècnica de Catalunya, Avinguda Doctor Marañón 44, E-08028 Barcelona, Spain

E-mail: jmsancho@ecm.ub.es

Abstract
Particles moving on perfect periodic surfaces under the influence of external forces may move along directions that deviate from that of the force. We briefly recall previous results for transport of particles on surfaces with *periodic traps* or *periodic obstacles* driven by a constant external force, and present new results for particles moving in a *harmonic periodic potential*. The sorting properties are explored as a function of a number of control parameters, specifically the friction, force amplitude and direction, temperature, and lattice constants.

(Some figures in this article are in colour only in the electronic version)

1. Introduction

Diffusion processes of passive particles, viewed as the erratic motion of particles caused by finite temperatures, were documented more than a century ago by Brown [1], and continue to attract wide interest. The seminal work of Einstein [2] relating macroscopic transport and diffusion to the microscopic structure of matter was the starting point of research that has never abated. Transport (i.e., average motion) is a direct result of deterministic Newtonian dynamics, but random motion is a natural consequence of the temperature as a prime source of disorder. Einstein's approach, based on the derivation of an equation for the probability density of the velocity of a particle, inspired Langevin's derivation of a more familiar Newtonian mechanical scenario incorporating a friction term complemented with a stochastic force [3]. Careful experiments confirmed the theoretical predictions [4].

Nowadays the rich phenomenology of transport of particles on crystalline surfaces is attracting enormous interest for its technological relevance at scales ranging from the atomic

___

[4] Author to whom any correspondence should be addressed.

and molecular to the colloidal and even the cellular. The advance of nanoscopic technologies such as the scanning tunnelling microscope (STM) has made it possible experimentally to follow the random motion of single particles or molecules on surfaces [5]. Over the past few years, interest in the transport properties of Brownian particles on solid surfaces has flourished and has included adsorbates on crystal surfaces [6], sorting of colloidal spheres [7–9] and of DNA macromolecules [10], polymer diffusion at interfaces [12], dimers of Si on a Si(100) surface [13, 14], long random jumps of organic molecules on a Cu(110) surface [15], and anomalous diffusion [16, 17] of gold nanoclusters on graphite planes [18] and in intracellular transport [19].

Of the very rich variety of transport problems, here we focus on sorting phenomena when particles in a thermal bath and in the presence of an external force or field flow move on a surface modelled by a two dimensional periodic potential. This work is motivated by recent experiments in colloidal transport in a periodic potential landscape generated with an array of optical tweezers [7–9], or via microfabricated technology to create an array of obstacles [10].

It is now possible to create a landscape with multiple traps or wells of any geometry (periodic or random) with the use of diffractive optical elements to build holographic tweezers [7–9]. The hologram (phase modulated pattern) for a particular distribution of wells is generated by a computer and etched on a glass plate using standard lithographic procedures. Dynamical holograms are also possible. A hologram of optical traps can produce a surface to which colloidal particles respond as would atoms to a crystalline surface structure. The parameters of these wells such as their width and depth are also controlled. Thus one can study transport properties of mesoscopic particles in a well-controlled scenario in which individual particles can be tracked. These ideas have been applied to the transport of colloidal spheres [7–9]. An alternative technique consists of the creation of periodic obstacles on a surface by microfabricated technology. DNA fragments [10] or disperse microspheres [11] in a fluid are then drifted across the surface by a forced laminar flow.

One of the outcomes of these experiments in the case of wells (traps) and also in the case of obstacles is the phenomenon of sorting [7–11, 20, 21]. A static array of wells or of obstacles can be used to sort a mixture of particles drifted by a steady fluid flow or an external force field. Particles are deflected with respect to the main streaming direction according to some individual characteristic of the particles (size, index of refraction, etc). It has been seen in these experiments that some particles are strongly deflected from the flow trajectory, others are less deflected, and some do not change their direction at all. As a result, an ensemble of different particles segregates in different directions and can be collected at different angles in the output flow. In the optical experiments a set of wells or traps is generated according to a desired spatial symmetry [7–9]. Here the particles move from one well to another over the intermediate plateaus. The wells 'compete' with the external force and cause the particles to move along directions that may not coincide with that of the force. The role of fluctuations in these experiments is especially relevant if the external force is not strong enough to prevent trapping in the potential wells, in which the particles would remain forever in the absence of thermal fluctuations. If the force is sufficiently strong and, in general, in the microfabricated obstacle technology where impenetrable obstacles (cylindrical towers) deviate the particle trajectories, the role of fluctuations is less crucial [10, 11]. Different configurations of obstacles as well as obstacle asymmetry have been used to enhance the sorting capability.

The sorting phenomenon is generic and will occur for any periodic configuration of wells and obstacles. In particular, in this paper we extend earlier work and explore its occurrence with a simple harmonic potential with both maxima and minima. Our scenario is an ensemble of non-interacting classical Brownian particles of mass m obeying a standard Langevin equation in the presence of thermal noise and its associated Stokes friction. Particles feel a two-dimensional

periodic potential with two lattice constants λ_x and λ_y, and are driven by a constant force of variable direction. This scenario corresponds to the canonical ensemble with a Boltzmann equilibrium distribution.

In section 2 we introduce the principal equations of our approach, briefly review our results for traps and obstacles, and specify the harmonic potential to be used to generate our new results. In section 3 we present our numerical results for symmetric and asymmetric lattices with harmonic potentials. We end in section 4 with some conclusions and perspectives.

2. Periodic potentials

We start with the equations of motion for the components (x, y) of the particle position on a surface,

$$
\begin{aligned}
m\ddot{x} &= -\frac{\partial}{\partial x} V\left(\frac{x}{\lambda_x}, \frac{y}{\lambda_y}\right) - \mu\dot{x} + f_x + \xi_x(t) \\
m\ddot{y} &= -\frac{\partial}{\partial y} V\left(\frac{x}{\lambda_x}, \frac{y}{\lambda_y}\right) - \mu\dot{y} + f_y + \xi_y(t).
\end{aligned}
\tag{1}
$$

Here $V(x/\lambda_x, y/\lambda_y) = V_0 \mathcal{V}(x/\lambda_x, y/\lambda_y)$ is a periodic potential of height or depth V_0 ($\mathcal{V}$ is a potential of unit height or depth), and a dot denotes a derivative with respect to t. The parameters λ_x and λ_y are characteristic lengths, the f_i are the Cartesian components of the constant external force whose magnitude is $f_0 = \sqrt{f_x^2 + f_y^2}$, the parameter μ is the phenomenological coefficient of Stokes friction, and the $\xi_i(t)$ are mutually uncorrelated white (thermal) noises that obey the equilibrium fluctuation–dissipation relation,

$$
\langle \xi_i(t)\xi_j(t')\rangle = 2\mu k_B T \delta_{ij}\delta(t - t').
\tag{2}
$$

The transformation of variables

$$
r_x = \frac{x}{\lambda_x}, \qquad r_y = \frac{y}{\lambda_x}, \qquad \tau = \sqrt{\frac{V_0}{m}}\frac{t}{\lambda_x},
\tag{3}
$$

leads to transformed Langevin equations in terms of dimensionless variables,

$$
\begin{aligned}
\ddot{r}_x &= -\frac{\partial}{\partial r_x}\mathcal{V}(r_x, r_y/a) - \gamma\dot{r}_x + F_x + \zeta_x(\tau), \\
\ddot{r}_y &= -\frac{\partial}{\partial r_y}\mathcal{V}(r_x, r_y/a) - \gamma\dot{r}_y + F_y + \zeta_y(\tau),
\end{aligned}
\tag{4}
$$

where $a = \lambda_y/\lambda_x$, and the noise terms obey the fluctuation–dissipation relation

$$
\langle \zeta_i(\tau)\zeta_j(\tau')\rangle = 2\gamma\mathcal{T}\delta_{ij}\delta(\tau - \tau').
\tag{5}
$$

In addition to lattice geometry parameters, the independent (dimensionless scaled) parameters of the problem are the temperature $\mathcal{T}$, the dissipation γ, the magnitude F_0 of the external force,

$$
\mathcal{T} = k_B T/V_0, \qquad \gamma = \mu\lambda_x/\sqrt{mV_0}, \qquad F_0 = \frac{\lambda_x f_0}{V_0},
\tag{6}
$$

and the angle θ between the external force and the x axis. Our interest lies in the mean particle velocity $\langle v \rangle$ as a function of these parameters.

For any given potential, our numerical simulations yield the Cartesian components of the average velocity,

$$
\langle v_i \rangle = \lim_{\tau \to \infty} \frac{\langle r_i(t)\rangle}{\tau},
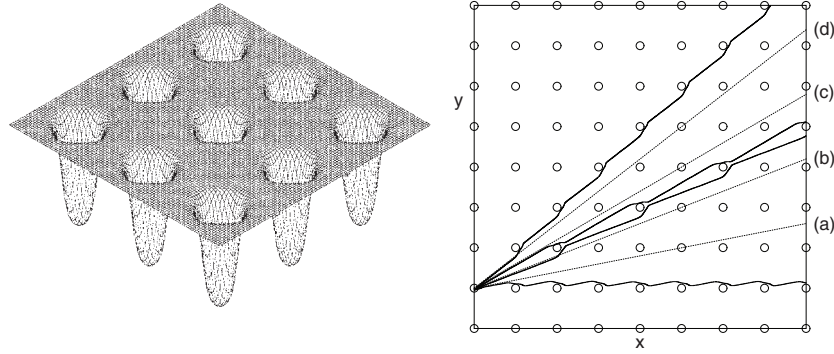\tag{7}
$$

Figure 1. Left panel: a finite portion of a two-dimensional potential with periodically located traps (wells) of depth V_0 connected by flat plateaus. Right panel: particle trajectories for forces applied at different angles represented by the dotted lines. Parameter values are $A = 5$, $B = 0.7$, $\mathcal{T} = 10^{-4}$, $\gamma = 20$, $F_0 = 8$. From [21].

from which we construct the components parallel and perpendicular to the force $\boldsymbol{F}$:

$$\langle v_\parallel \rangle = \langle v_x \rangle \cos\theta + \langle v_y \rangle \sin\theta, \qquad \langle v_\perp \rangle = -\langle v_x \rangle \sin\theta + \langle v_y \rangle \cos\theta. \tag{8}$$

The magnitude of the deviation of the direction of the average particle velocity from that of the force can be characterized by either of the angles α (called the deflection angle) and $\psi = \alpha + \theta$ (called the velocity angle), defined as

$$\tan\alpha = \frac{\langle v_\perp \rangle}{\langle v_\parallel \rangle}, \qquad \tan\psi = \frac{\langle v_y \rangle}{\langle v_x \rangle}. \tag{9}$$

In [21] we focused on an array of wells or obstacles separated by plateaus, modelled by the potential (with $\lambda_x = \lambda_y \equiv \lambda$)

$$V\left(\frac{x}{\lambda}, \frac{y}{\lambda}\right) = \frac{\pm V_0}{1 + \mathrm{e}^{-g(x,y)}}, \tag{10}$$

where $g(x, y)$ is the periodic two-dimensional function

$$g(x, y) = A\left[\cos\left(2\pi x/\lambda\right) + \cos\left(2\pi y/\lambda\right) - 2B\right]. \tag{11}$$

The parameter V_0 controls the depth or height of wells or obstacles, A controls the steepness of these features, and B determines the relative size of a well or obstacle with respect to the spatial period λ. The potential in the case of wells is illustrated in the left panel of figure 1, as are typical particle trajectories in this potential in the right panel. The parameter B can be associated with the size of the diffusing particle; larger values of B lead to shallower and narrower wells and are therefore associated with larger particles. The potential and associated trajectories in the case of obstacles are shown in figure 2.

We exhibit two particularly important simulation results, specifically obtained previously for the case of wells [21] but qualitatively very similar for the case of obstacles. One, shown in figure 3, shows the deflection angle α versus the direction of the force, and is important because it demonstrates that there is a direction of the force that leads to maximal deviation of α from zero for a given particle size, while other force directions also lead to pronounced but smaller deviations. It is also clear that the optimal angle for sorting depends on the sizes of the particles to be sorted. In the case of wells (but not of obstacles) with increasing temperature the trajectories become more erratic as thermal fluctuations agitate the particles away from the direction of the force and of the nearest wells. As seen in the lower panel of the figure,
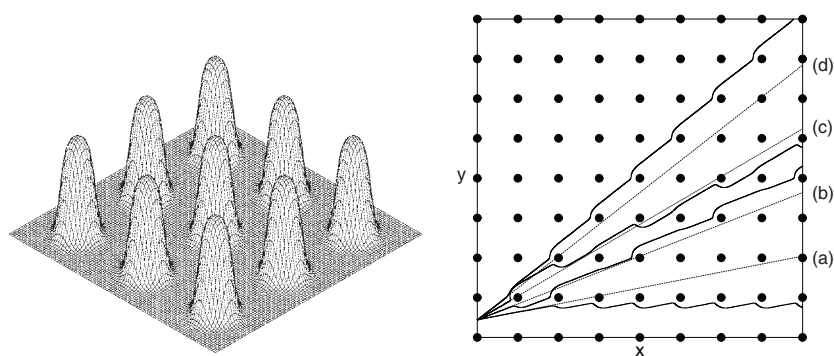
Figure 2. Left panel: a finite portion of a two-dimensional potential with periodically located obstacles of height V_0 connected by flat plateaus. Right panel: typical particle trajectories for forces applied at different angles represented by the dotted lines. Parameter values as in figure 1.
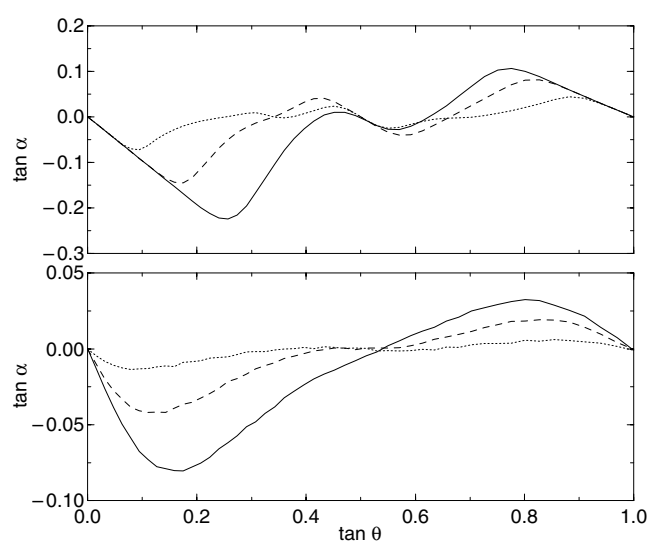

Figure 3. Deflection angle versus field direction for the case of potential wells separated by plateaus, for $F_0 = 8$, $\gamma = 20$, different values of the potential parameter B (increasing B is associated with increasing particle size), and two temperatures. Upper panel, $\mathcal{T} = 0.01$; lower panel, $\mathcal{T} = 0.1$. Data correspond to $B_1 = 0.5$ (solid lines), $B_2 = 0.7$ (dashed lines) and $B_3 = 0.9$ (dotted lines). From [21].

the deflection angle is now smaller than before, but there is still an angle θ for maximum deviation from $\alpha = 0$ that varies with particle size. This figure compares favourably not only qualitatively but even quantitatively with figure 4 of [7]. At sufficiently high temperature the effect disappears as the wells become irrelevant.

The other result, shown in figure 4, is a terrace phenomenon in the dependence of the absolute velocity angle on the direction of the force. This phenomenon was first predicted in [20] and has since been observed and discussed extensively [7, 8] (see figure 5 in [7] and figures 2 and 3 in [8]). The terrace steps have been called 'kinetically locked-in states' and can be understood on the basis of the trajectories in figures 1 and 2. All the trajectories included in a small cone pointing toward a particular well will emerge out of this well within an identical
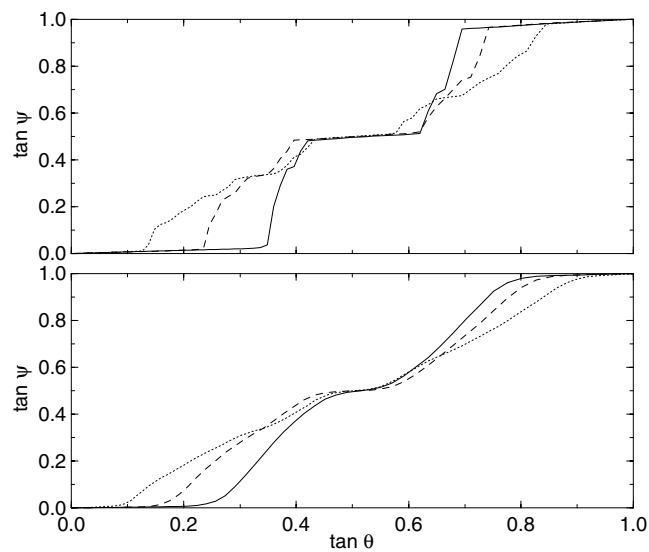
Figure 4. Terraces in the absolute velocity angle for a surface of potential wells separated by plateaus, for $F_0 = 8$, different values of the parameter B, and two temperatures. Upper panel $\mathcal{T} = 10^{-4}$, lower panel $\mathcal{T} = 10^{-2}$. Data correspond to $B = 0.5$ (solid lines), 0.7 (dashed lines), and 0.9 (dotted lines). From [21].

cone, as illustrated by the cone between lines (b) and (c) in the figures. In the case of wells, the terraces are clearly pronounced at low temperatures, but as the temperature increases the particle agitation disturbs and washes out the smaller cones (this corresponds to the notion of 'statistically locked-in transport' in [8]), leading to the eventual disappearance of the terraces. Understandably, the terraces are more pronounced for smaller particles.

In our new work we focus on surfaces described by the following generic two-dimensional periodic potential:

$$V(x, y) = V_0 \, \mathcal{V}\left(\frac{x}{\lambda_x}, \frac{y}{\lambda_y}\right) = \frac{V_0}{2}\left[\cos\left(\frac{2\pi x}{\lambda_x}\right) + \cos\left(\frac{2\pi y}{\lambda_y}\right)\right], \qquad (12)$$

where V_0 is the barrier height at the saddle points, and the ratio $\lambda_y/\lambda_x \equiv a$ characterizes the symmetry of the potential (square when $a = 1$). The two potential symmetries used here are shown in figure 5 along with some examples of particle trajectories. Further simulation results for this potential are presented in the next section.

3. Numerical results

We start with some observations about the trajectories in figure 5. Note that the particles are attracted to each nearby potential well encountered as the particle moves along. Similarly, each potential maximum deflects the particle along its journey. Both of these lead to deviations from motion along the direction of the force. The trajectories shown here correspond to a high value of the friction.

Typical deviation angles for the trajectories are plotted in figure 6. The deviations in the square potential are symmetric about the diagonal (at $\theta = \pi/4$ the particles follow the direction of the force). For the asymmetric potential this is not the case, and indeed there is moderate sorting when the force lies along the diagonal ($a = \sqrt{2}$ puts the diagonal at $\tan\theta = \sqrt{2}$ so that $\theta \approx 55°$). In this lattice there is no sorting at $\tan\theta = 1/\sqrt{2}$ ($\theta \approx 35°$), that is, when the force
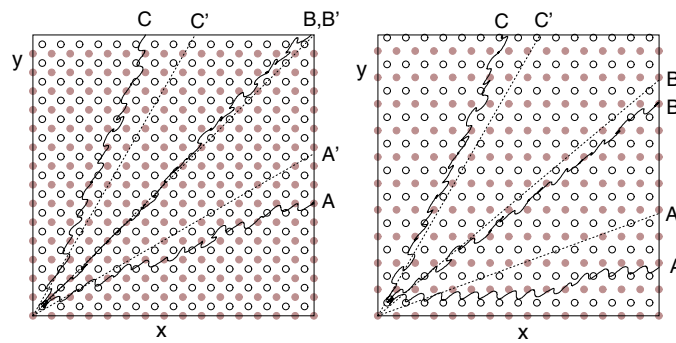
Figure 5. Surface plots of the potentials (12) showing several trajectories. The open circles are the locations of the minima and the solid circles indicate the maxima. Left panel: symmetric potential; the pairs (A′, A), (B′, B), etc indicate the direction of the force and the associated particle trajectory. $\theta = \pi/6$ (A, A′), $\theta = \pi/4$ (B, B′), and $\theta = \pi/3$ (C, C′). Right panel: asymmetric potential for $a = \sqrt{2}$; $\theta = \pi/9$ (A, A′), $\theta = 2\pi/9$ (B, B′), and $\theta = \pi/3$ (C, C′). Parameter values: $F_0 = 6$, $\mathcal{T} = 0.01$ and $\gamma = 10$.
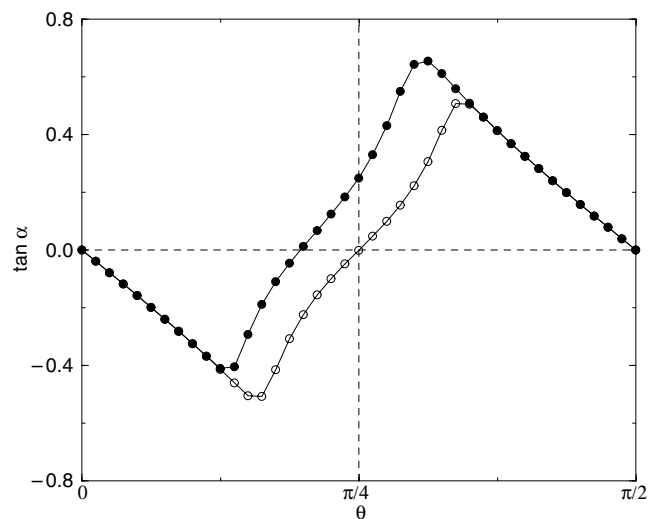

Figure 6. $\tan\alpha$ versus θ for the symmetric (open symbols, $F_0 = 6$) and asymmetric (solid symbols, $F_0 = 5$) potentials. Other parameters: $\gamma = 10$, and $\mathcal{T} = 0.01$.

is perpendicular to the diagonal. Along this direction one observes a 'dynamical symmetry': as the particle advances, there is an alternating spatial asymmetry that causes the particle to zigzag around the direction of the force so that on average its trajectory lies along this direction. The forces chosen for the two geometries in the plot are different for reasons that will become clear subsequently. The effect of friction for both lattices is illustrated in figure 7. While one must be cautious about comparisons in absolute behaviour because the two curves correspond to different parameter values and different geometries, the general qualitative behaviour is the same for both. In both lattices, inertial effects lead to persistence in the direction of the motion and thus contribute to the tendency of the particles to follow the direction of the force. The deflection angle therefore increases with increasing friction, and saturates when the inertial contributions no longer play a role. The largest deviation is obtained for particles with high
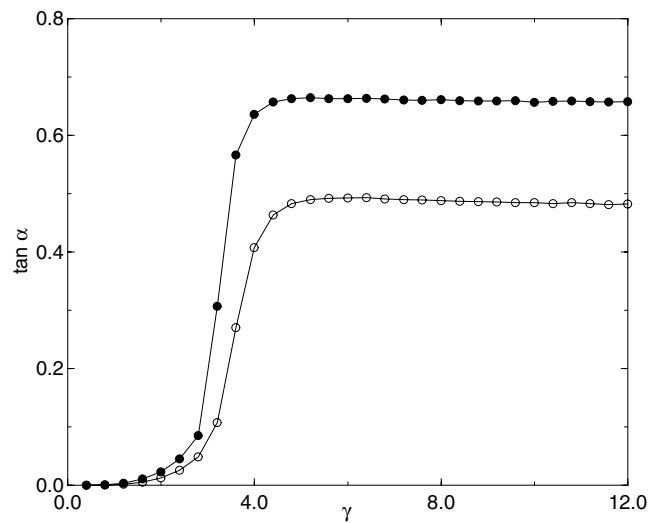
Figure 7. $\tan \alpha$ versus γ for the symmetric (open symbols) and asymmetric (solid symbols) potentials. For the symmetric potential the parameters are $F_0 = 6$ and $\theta = \pi/3$ ($\tan \theta = 1.732$). For the asymmetric potential $F_0 = 5$ and $\tan \theta = \sqrt{2}$. For both, $\mathcal{T} = 0.01$.
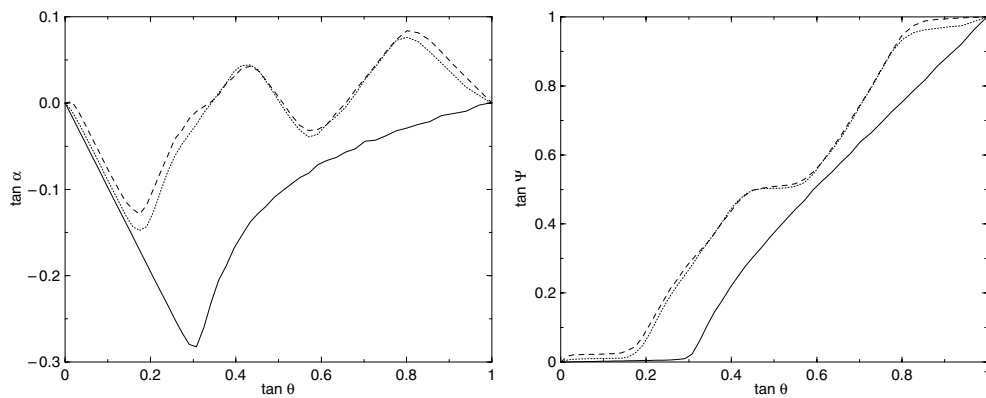

Figure 8. Left panel: $\tan \alpha$ versus $\tan \theta$. Right panel: $\tan \Psi$ versus $\tan \theta$. Parameters in both panels: $\gamma = 20$, $F_0 = 10$, $\mathcal{T} = 0.01$, and for two of the potentials, $A = 5$ and $B = 0.7$. Solid curves, periodic potential considered in this paper; dashed curves, potential with wells and flat plateaus; dotted curves, potential with obstacles.

friction. On the other hand, particles with high friction are not effectively sorted on the basis of their friction because they are all deflected equally.

It is also interesting to compare the sorting capability of the systems considered in our earlier work with that of the periodic lattice of the same symmetry (square) as considered here, at least for some specific parameter values. Such a comparison is shown in the two panels of figure 8. The sorting as measured by the angle α is very similar for the two potentials considered in our previous work but distinctly more effective for the simple harmonic periodic potential introduced in this paper.

To assess the sorting capabilities of our surfaces it is useful to focus on the dependence of the trajectories on θ, F_0, and γ. The first two will yield information on the externally
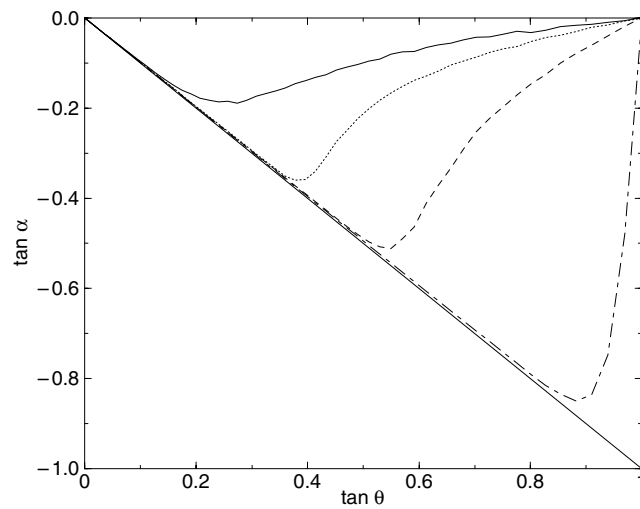
Figure 9. $\tan \alpha$ versus $\tan \theta$ in a square lattice for four forces: $F_0 = 10$ (solid), 8 (dotted), 6 (dashed) and 4 (dot–dashed). Other parameters: $\gamma = 10$ and $\mathcal{T} = 0.01$.
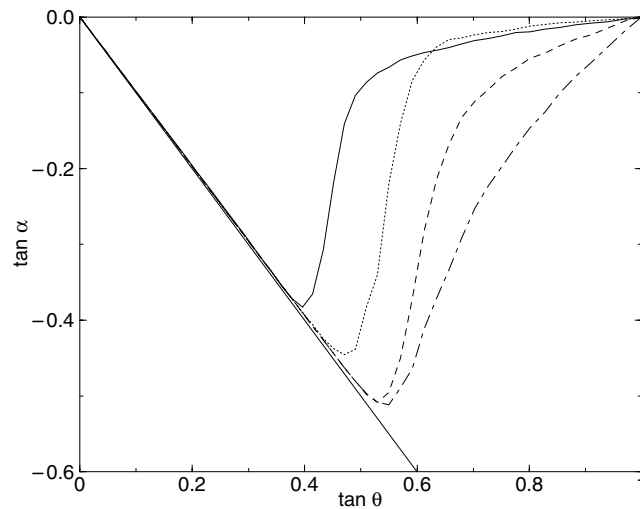

Figure 10. $\tan \alpha$ versus $\tan \theta$ for four values of the friction parameter: $\gamma = 0.4$ (solid), 2 (dotted), 4 (dashed), and 10 (dot–dashed). Other parameters: $F_0 = 6$ and $\mathcal{T} = 0.01$.

controllable parameters, and the third on the particle sorting capability of the potential on the basis of the friction coefficient as the differentiating feature.

In figure 9 we present the deviation angle as a function of the direction of the force for the square lattice. The deviation is zero (particles move in the direction of the force) when $\theta = 0$ and, as noted earlier, also when $\theta = \pi/4$ ($\tan \theta = 1$). As θ increases from zero, the particles continue to move along the x axis (indicated by the diagonal line in the figure). The deviation angle reaches a maximum at an angle that decreases with increasing F_0 (a stronger force is better able to pull the particles along its direction). Note that the deviation angle becomes quite sizable. Figure 10 shows the deviation angle as a function of the direction of the force
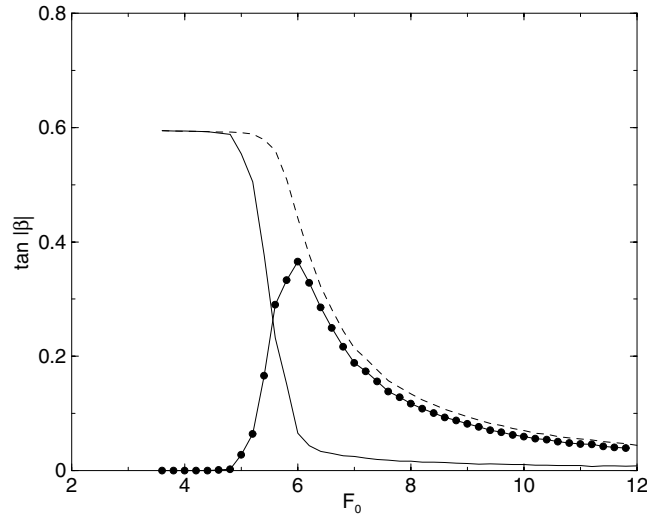
Figure 11. Sorting of particles with different friction coefficients when $\theta = \pi/3$ in the symmetric potential. The β on the vertical axis is different for each curve: $\beta = \alpha_1$ for $\gamma = 2$ (solid line), $\beta = \alpha_2$ for $\gamma = 10$ (dashed line), and $\beta = \alpha_1 - \alpha_2$ (full circles). The temperature is $\mathcal{T} = 0.01$.

for different friction coefficients. Again, at small angles the particle moves along the x axis. At large θ (near $\pi/4$), the particle moves nearly in the direction of the force, more so for lower friction. The deviation angle varies rapidly with θ over a narrow range of θ.

Of particular interest for sorting is the difference in the deviation angle of different particles. Figure 10 shows that if friction is the sorting parameter, this difference is greatest for $0.4 \lesssim \tan\theta \lesssim 0.6$ for the parameter values used in the figure. Figure 11 quantifies the sorting behaviour more clearly by showing the difference in the deviation angles of two particles with different friction coefficients as a function of the magnitude of the force. The maximum occurs at $F_0 \approx 6$, in agreement with the maximum deviation seen in figure 10 for the parameter values indicated in the caption of figure 11. The maximum becomes less pronounced (sorting becomes more difficult) and shifts to smaller values of $\tan\theta$ with increasing temperature; see figure 12.

The sorting capabilities of the asymmetric potential surface are similar to those of the symmetric surface but for different values of the control parameters. In figure 13 we show the results comparable to those of figure 11, but now the optimal sorting occurs at a smaller value of the force, $F_0 \sim 5$. Recall that in figures 6 and 7 we chose different forces to illustrate the trajectory deviations for the two lattices. Now we see that these forces were chosen to correspond to the optimal forces for sorting for each of the lattice geometries.

4. Conclusions and perspectives

We have investigated sorting phenomena of an ensemble of particles in two-dimensional symmetric and asymmetric harmonic potentials subject to thermal fluctuations and external forces.

We have observed that the particle trajectories deviate from the direction of the external force by angles that depend on the symmetry of the lattice, the magnitude and direction of the external force, and the friction coefficient of the particles, and we have found larger deviations in the harmonic potentials than those observed in other potentials used in recent experiments.
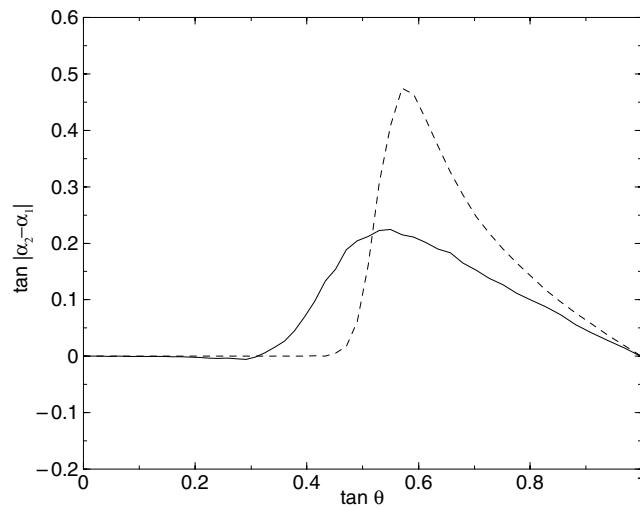
Figure 12. Sorting for a symmetric potential as measured by $|\alpha_2 - \alpha_1|$ for two temperatures: $\mathcal{T} = 0.1$ (solid) and $\mathcal{T} = 0.01$ (dashed). Parameters: $\gamma_1 = 10$, $\gamma_2 = 2$, and $F_0 = 6$.
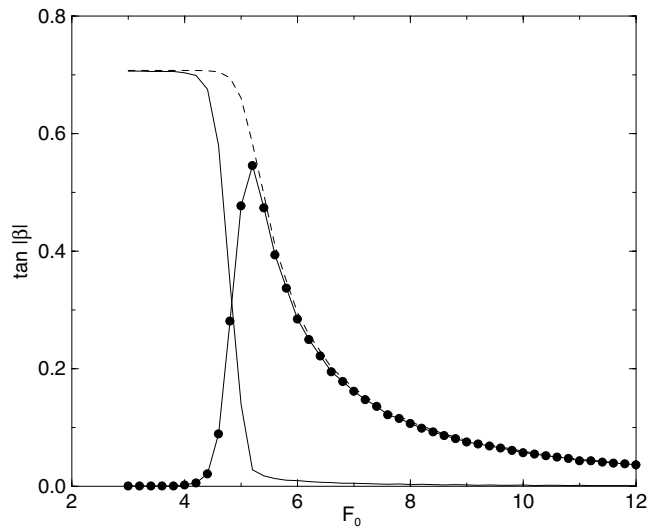

Figure 13. Sorting of particles with different friction coefficients when $\tan\theta = \sqrt{2}$ in the asymmetric potential. The β on the vertical axis is different for each curve: $\beta = \alpha_1$ for $\gamma = 2$ (solid line), $\beta = \alpha_2$ for $\gamma = 10$ (dashed line), and $\beta = \alpha_1 - \alpha_2$ (full circles). The temperature is $\mathcal{T} = 0.01$.

We find that the symmetry of the harmonic potential does not affect the sorting behaviour in any essential way, and that one can adjust force parameters so that symmetric and asymmetric surfaces lead to the same sorting effectiveness. We also note that sorting is principally a deterministic phenomenon even in the presence of diffusion provided the temperature is not too high.

We investigated in some detail whether particles of different friction coefficients can be sorted in this way. We have shown that it is indeed possible to do so in appropriate parameter
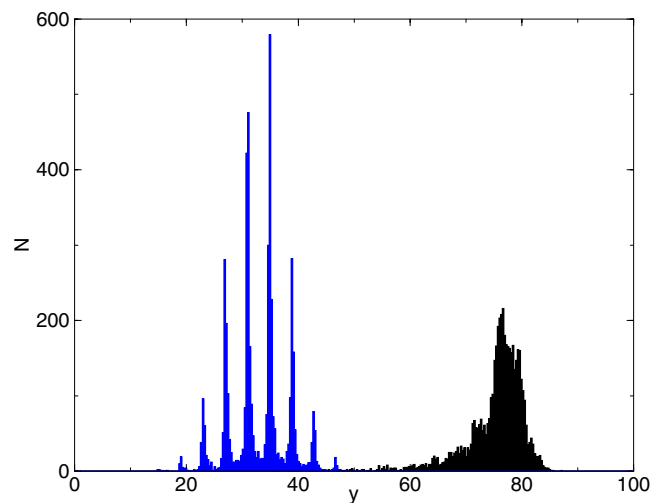
Figure 14. Un-normalized histograms of the y-position of 5000 particles collected at $x = 120$ for $\gamma_1 = 10$ (lower multimodal distribution) and $\gamma_2 = 2$ (upper unimodal distribution). Other parameters: $\tan(\theta) = 0.65$, $F_0 = 6$ and $\mathcal{T} = 0.01$.

regimes, and specifically illustrate this capability once again in figure 14. Here a sharp initial distribution of two sets of particles, each set characterized by a different friction coefficient, is clearly segregated when they arrive at the other end of our lattice. We see in this figure that the output distribution for the smaller friction is essentially monomodal on the scale of the figure, while that of the particles with the larger friction is spatially multimodal with maxima separated by the spatial period λ, but that one set of particles is clearly separated from the other set.

Acknowledgments

References

[1] Brown R 1828 *Edinb. New Phil. J.* **5** 358
[2] Einstein A 1905 *Ann. Phys., Lpz.* **17** 549
[3] Langevin P 1908 *C. R. Acad. Sci. Paris* **146** 530
[4] Perrin J B 1909 *Ann. Chim. Phys.* VIII **18** 5
[5] Swartzentruber B S 1996 *Phys. Rev. Lett.* **76** 459
[6] Hershkovitz E, Talkner P, Pollak E and Georgevskii Y 1999 *Surf. Sci.* **421** 73
[7] Korda P T, Taylor M B and Grier D G 2002 *Phys. Rev. Lett.* **89** 128301
[8] Gopinathan A and Grier D G 2004 *Phys. Rev. Lett.* **92** 130602
[9] MacDonald M P, Spalding G C and Dholakla K 2003 *Nature* **426** 421
[10] Huang L R, Cox E C, Austin R H and Sturm J C 2004 *Science* **304** 987
[11] Huang L R, Cox E C, Austin R H and Sturm J C 2003 *Anal. Chem.* **75** 6963
[12] Nixon G I and Slater G W 1996 *Phys. Rev.* E **53** 4969
[13] Swartzentruber B S, Smith A P and Jónsson H 1996 *Phys. Rev. Lett.* **76** 2518
[14] Romero A H, Lacasta A M and Sancho J M 2004 *Phys. Rev.* E **69** 051105
[15] Schunack M *et al* 2002 *Phys. Rev. Lett.* **88** 156102

[16] Sancho J M, Lacasta A M, Lindenberg K, Sokolov I M and Romero A H 2004 *Phys. Rev. Lett.* **92** 250601

[17] Lacasta A M, Sancho J M, Romero A H, Sokolov I M and Lindenberg K 2004 *Phys. Rev.* E **70** 051104

[18] Luedtke W D and Landman U 1999 *Phys. Rev. Lett.* **82** 3835

[19] Suh J, Wirtz D and Hanes J 2003 *Proc. Natl Acad. Sci. USA* **100** 3878

[20] Reichhardt C and Nori F 1999 *Phys. Rev. Lett.* **82** 414
Reichhardt C and Olson Reichardt C J 2004 *Phys. Rev.* E **69** 041405
Reichhardt C and Olson Reichardt C J 2004 *Europhys. Lett.* **68** 303

[21] Lacasta A M, Sancho J M, Romero A H and Lindenberg K 2004 *Phys. Rev. Lett.* **94** 160601